Energy Engineering

Tech Science Press

https://doi.org/10.32604/ee.2026.074998

ARTICLE

Dynamic Energy Management in a Hybrid Microgrid Integrating PV, Wind, Fuel Cell and EV Battery Using Fuzzy Logic Control

Jawad Hameed*, Jiefeng Hu, Md Liton Hossain and Syed Islam

Centre for New Energy Transition Research, Federation University Australia, Mount Helen, Ballarat, Australia

*Corresponding Author: Jawad Hameed. Email: jhameed@students.federation.edu.au

Received: 23 October 2025; Accepted: 11 March 2026; Published: 27 May 2026

ABSTRACT: This paper presents a dynamic energy management strategy for a community-scale campus hybrid microgrid integrating photovoltaic (PV) generation, aggregated wind power, a proton exchange membrane fuel cell, and battery energy storage to support electric vehicle (EV) charging infrastructure under variable environmental and load conditions. The system configuration is inspired by existing renewable energy installations and planned developments at the Federation University Mt Helen Campus, enabling realistic modeling of aggregated demand and coordinated multi-source operation. To enhance physical realism, power electronic conversion efficiencies and hierarchical control dynamics are incorporated, while the wind subsystem is represented using an aggregated generation model consistent with MW-scale operation. The proposed control architecture employs a Mamdani-type fuzzy logic controller (FLC) to coordinate distributed energy resources in real time based on solar irradiance, temperature, wind speed, load demand, and battery state of charge. A comprehensive MATLAB/Simulink model interfaces each source through converter-based power electronic stages, enabling adaptive power flow and stable system operation. Simulation results demonstrate uninterrupted load supply, reduced grid dependency, and effective bidirectional energy exchange. PV output varies between 18.76 and 95.12 kW, wind generation ranges from 1553.5 to 6493.84 kW, and the fuel cell provides a stable 1000 kW contribution, while the battery dynamically supports charging and discharging up to 203.07 kW. Power balance analysis confirms coordinated load sharing among all sources, with the grid supplying or absorbing power as required. Quantitative comparison with conventional PI-based dispatch demonstrates improved transient response, enhanced voltage regulation, smoother control effort, and improved power balance stability, with peak system efficiency reaching 97.83%, validating the proposed EMS as a robust and adaptive solution for EV-integrated renewable microgrids and next-generation smart energy systems.

KEYWORDS: Hybrid microgrid; fuzzy logic control; renewable energy integration; dynamic load; battery storage; PV system; wind turbine; fuel cell

1 Introduction

Modern energy problems can be revolutionized by hybrid microgrids, which allow energy storage devices and a variety of renewable energy sources to be integrated to satisfy fluctuating load demands. A lot of research has been done on microgrids that combine biomass, wind turbines, and solar photovoltaics to lessen reliance on fossil fuels, particularly for power in rural areas. Power quality issues, voltage and frequency instability, and intermittent generation pose challenges to these environmentally sustainable systems [1]. To ensure reliable operation, advanced energy management strategies are required to stabilize hybrid configurations under dynamic conditions. Isolated microgrids commonly rely on hybrid wind and solar configurations managed through DFIG-based systems and battery banks. These use MPPT control and

vector-based indirect control, sometimes enhanced by droop characteristics for frequency regulation based on battery state of charge. Simulation and experimental validations show such systems can maintain performance under component unavailability or nonlinear load conditions [2]. Cooperative energy sharing among several microgrids is presented in [3] as a substitute to reduce intermittency, particularly when backed by dispersed energy storage. Algorithms for online and offline energy management are presented to maximize efficiency and minimize expenses. These methods, however, do not prioritize real-time coordination based on fuzzy logic, which can provide greater flexibility. By utilizing G2V and V2G technologies, EVs are being utilized more and more as dynamic energy storage units in microgrids. A planning algorithm was proposed in [4] to optimize EV charging station deployment considering feed-in tariffs and state-of-charge scenarios. Results show significant economic and technical benefits, but effective integration still requires adaptive energy management methods that handle the uncertain EV participation.

Hybrid energy storage solutions using battery-supercapacitor combinations or hydrogen storage with solid oxide fuel cells have also been implemented to enhance wind energy utilization. In [5], a fuzzy enhanced direct reactive power control algorithm was used to manage fluctuations and improve output stability. Nonetheless, these systems benefit further from unified fuzzy logic-based supervisory control for all energy sources and storage. FLCs have been widely adopted to manage uncertainties and nonlinearities in microgrid operation. A standalone hybrid system combining wind, solar, fuel cell, and battery storage was experimentally validated in [6], using FLC dependent MPPT and SoC-based energy flow regulation. The system demonstrated robust voltage and frequency control for off-grid applications. In [7], a hybrid PV–fuel cell system for EV recharging was developed with mathematical modeling and fuzzy-based power management. Simulation results under varying conditions confirmed improved energy efficiency, though practical implementation calls for more scalable fuzzy rule bases. Fuzzy logic also enhances battery life and hydrogen efficiency in DC microgrids. In [8], a centralized EMS used sigmoidal FC control based on battery SoC and PV de-rating to avoid deep battery discharge, validated through hardware-in-loop testing. Such systems emphasize the role of fuzzy-based decision layers in centralized EMS structures.

Community-scale hybrid microgrids with excess PV capacity can benefit from intra-community energy sharing, as explored in [9]. Load leveling through shared fuel cell and battery systems was proposed to support EV charging infrastructure. While effective, these systems often lack adaptive control required for seamless shift among grid-linked and islanded modes. Economic dispatch and scheduling in grid-interactive microgrids have been explored using MPC methods in [10], enabling participation in energy markets and interaction with other agents. However, fuzzy-based EMS could offer better real-time adaptability with lower computational burden. Hybrid energy storage coordination using droop-based decentralized control has also been proposed in [11]. Here, multilevel EMS mitigates bus voltage deviations and enhances SoC balancing, showing that fuzzy logic can be layered into both primary and secondary control levels. A low-component multi-source converter architecture interfacing PV, wind, and HESS with fuzzy control was developed in [12], simplifying control and enhancing supercapacitor response to fast transients. This topology offers a promising base for deploying fuzzy energy dispatch logic across multiple storage tiers. In [13], fuzzy-integrated fractional-order controllers were applied for DC bus regulation and power balancing under fluctuating irradiance. Van der Pol oscillator-based virtual control further enhanced dynamic response. Still, rule optimization and fuzzy coordination remain critical under hybrid operation.

ANNs were used in [14] for MPPT tracking and power flow regulation in a hybrid scheme. A fuzzy-based EMS minimized grid power draw, validating the self-learning potential of such systems. However, the complexity of ANN training makes fuzzy controllers more suitable for adaptive real-time applications. Stochastic control methods based on Crow Search Algorithms and unscented transforms have been introduced for hybrid AC/DC microgrids in [15]. While these account for uncertainties in load and generation, fuzzy

controllers offer more intuitive implementation and faster real-time response. Rule-based EMS frameworks combined with optimization logic for PV–battery–diesel microgrids have been explored in [16]. These reduce operational costs and emissions but still require real-time adaptability, which fuzzy logic readily supports. Decentralized EMS for PV-integrated EV charging stations was investigated in [17]. A droop-controlled SoC-based strategy was used for power-sharing among storage banks, ensuring extended battery life. However, real-time prioritization still benefits from fuzzy rule integration. Benchmarking tools like GA-based (Genetic Algorithms) optimization proposed in [18] introduce optimal real-time control computations but are limited in scaling to systems with multiple hybrid energy storage units and complex load patterns—an area where fuzzy logic offers distinct advantages. Ref. [19] demonstrates the effectiveness of hybrid energy management strategies in improving energy optimization voltage stability. A risk-based optimization model was proposed in [20] to address RPG curtailment and load shedding in hybrid AC/DC microgrids. While precise and rigorous, such methods are computationally demanding, requiring fuzzy-based heuristics for quick response. A comprehensive review in [21] emphasized the growing importance of hybrid microgrid control approaches yet highlighted a research gap in fuzzy logic-based adaptive coordination, especially when integrating wind, fuel cell, and EV batteries. Finally, a centralized fuzzy-controlled EMU for a grid-tied campus-level hybrid microgrid was proposed in [22], enabling flexible mode transitions, voltage balancing, and energy cost minimization. Experimental validation confirmed the effectiveness of fuzzy logic in real-time dynamic energy management.

From the literature, it is evident that FLC have distinct advantages in microgrids, particularly for handling uncertainties in source generation and demand. Yet, no existing approach fully integrates PV, wind, fuel cells, and EV batteries in a single adaptive framework using fuzzy logic for real-time energy management under variable load conditions. Many studies are either source-specific or optimization-centric, lacking the low-complexity, real-time adaptability that fuzzy logic offers. This study addresses the identified research gaps by proposing a supervisory energy management framework tailored for community-scale hybrid microgrids. The main contributions of this work are:

- **Development of a fuzzy logic–based energy management system** capable of coordinating PV generation, aggregated wind power, fuel cell generation, and EV battery storage in real time under dynamically varying environmental and load conditions.
- **Design of a computationally efficient rule-based control strategy** that eliminates dependence on predictive models or training datasets, enabling real-time adaptability and robustness against system nonlinearities and renewable intermittency.
- **Integration of EV battery storage into hybrid microgrid dispatch**, enabling bidirectional energy exchange and enhanced load support within an aggregated campus-scale energy ecosystem.
- **Demonstration of improved dynamic performance and voltage regulation** through quantitative comparison with conventional PI-based dispatch strategies.
- **Validation of coordinated multi-source power sharing**, ensuring reduced grid dependency and improved renewable energy utilization under fluctuating operating conditions.

Unlike conventional optimization-based or predictive EMS approaches, the proposed framework employs a transparent fuzzy decision-making structure that enables adaptive real-time coordination without requiring extensive computational resources or forecast data. This makes the proposed method particularly suitable for community-scale hybrid microgrids where renewable variability, EV charging demand, and distributed generation interactions must be managed efficiently and reliably.

The paper is organized as follows: Section 2 details the modeling of the hybrid microgrid architecture, detailing the configuration and interaction of PV, wind, fuel cell, and EV battery components. Section 3 elaborates formulation of Energy management scheme. Section 4 presents the control approach of all the

input, Section 5 presents the proposed Fuzzy logic EMS, Section 6 presents the simulation framework, test case scenarios, and a comparative evaluation of the system's performance against conventional methods. Finally, Section 7 concludes the study by summarizing the main outcomes and outlining potential future research guidelines.

2 System Description

A hybrid energy system integrating multiple RES like PV, wind turbine, and fuel cell along with an EV battery and grid connection to supply residential and static loads was presented in Fig. 1.

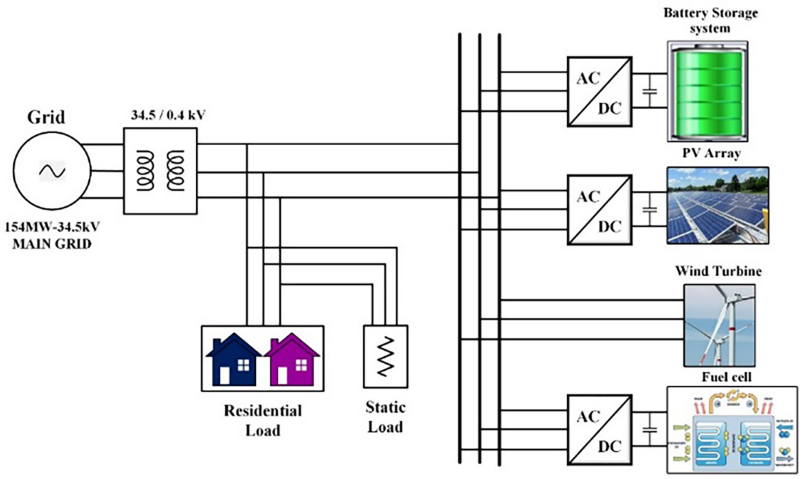

Figure 1: Proposed microgrid scheme.

The main grid delivers high-voltage AC power (154 MW at 34.5 kV), which is stepped down to 0.4 kV using a transformer for local distribution. The residential and static loads are connected at the low-voltage side. The PV array produces DC power, which is changed to AC using an AC-DC converter, and supports both local loads and EV battery charging. The EV battery operates as an energy storage unit and can store surplus energy or discharge when needed for load or grid support. The wind turbine is based on a DFIG configuration. The DFIG output undergoes AC-DC rectification, then passes through a boost converter, and is finally inverted back to AC for synchronized integration with the microgrid. This power conversion chain ensures regulated voltage and frequency compatibility with the grid. The fuel cell system produces DC power through electrochemical conversion of hydrogen, which is then fed into an AC-DC converter before integration. All these sources are coordinated via control electronics to maintain voltage stability, ensure optimal power flow, and support dynamic load conditions. This configuration exemplifies a modern smart microgrid where distributed generation, storage, and conversion systems work in tandem to meet varying energy demands and improve reliability. The modeling of the Proposed scheme is given as follows.

The generation and storage capacities used in this study are derived from real-world energy infrastructure and planned developments in the Ballarat region, rather than being arbitrarily selected. Specifically, the 6.5 MW wind capacity corresponds to the rated generation capacity of the Chepstowe Wind Farm in Ballarat, Victoria [1]. The approximately 95 kW photovoltaic (PV) array reflects the installed solar generation capacity at Federation University's Mt Helen Campus in Ballarat as shown in Fig. 2a. Furthermore, strategic development plans at the campus include the proposed installation of a 1 MW fuel cell system to support clean energy integration and enhance microgrid resilience. The 200-kW battery energy storage system has been installed too at Federation University's Mt Helen Campus in Ballarat to provide operational

flexibility, enable energy balancing between intermittent renewable sources and load demand, and support dynamic energy management within the hybrid microgrid as shown in Fig. 2b. Inverter interface, and associated power conversion equipment supporting the campus microgrid testbed can be seen from Fig. 2c,d.

Figure 2: Installed renewable energy and storage infrastructure at the Federation University Mt Helen Campus. (**a**) photovoltaic (PV) distribution and protection panels interfacing the solar generation system, (**b**) battery energy storage system cabinets used for energy storage and load support, (**c**) power electronic inverter unit responsible for DC–AC conversion and grid synchronization, and (**d**) auxiliary power conversion and monitoring equipment integrated within the campus renewable energy system.

In practical MW-scale hybrid microgrids, power electronic interfaces introduce non-negligible conversion losses. To enhance modelling realism and address idealized assumptions, efficiency factors are incorporated for each distributed energy resource (DER) interface in the proposed system.

Each subsystem is interfaced to the AC microgrid through rectifier–inverter or DC–DC conversion stages. The actual delivered power is therefore modelled as:

$$P_{out} = \eta \, P_{in} \tag{1}$$

where η represents the conversion efficiency of the respective power electronic stage.

2.1 Solar PV Design

In the proposed system, a high-efficiency SunPower SPR-415E-WHT-D PV module is modeled by the single-diode equivalent circuit to replicate nonlinear I–V behavior under dynamic environmental conditions. The array structure consists of 7 modules in series and 35 strings in parallel, optimized for stable voltage and current delivery, parameters of which can be seen from Table 1. The power output is simulated based on irradiance and temperature input. The I–V equation of the PV cell is given by Eq. (1),

$$I_{oc} = I_{PL} - I_{DS}\left(e^{\frac{q(V_T+IR_s)}{nkT}} - 1\right) - \frac{V + IR_{se}}{R_{sh}} \tag{2}$$

where, I_{oc} is Output current, V_T is Terminal voltage, I_{PL} is photo-generated current, I_{DS} is Diode saturation current (A), q is Electron charge, k is Boltzmann's constant, T is Temperature, R_{se} & R_{sh} is Series & shunt resistance, n is Ideality factor.

Table 1: Parametrs of PV panel.

Parameter	Value
Module	SunPowerSPR-415E-WHT-D
Maximum Power (W)	414.8
Open Circuit Voltage V_{oc} (V)	85.3 V
Short Circuit Current I_{sc} (A)	6.09 A
Voltage at MPP V_{mp} (V)	72.9 V
Current at MPP I_{mp} (V)	5.69 A
Diode Ideality Factor (n)	0.87223
Diode Saturation Current I_{DS} (A)	7.1698e−13
Shunt Resistance R_{sh}	419.78 Ω
Temperature Coefficient (%/°C)	−0.229

The grid-connected inverter efficiency for the PV system is modeled as:

$$\boldsymbol{P_{PV,actual} = \eta_{PV} P_{PV}} \tag{3}$$

*w*here, $\boldsymbol{\eta_{PV}} = 0.97$ represents typical high-efficiency three-phase *PV* inverters used in commercial installations.

2.2 Wind Model

In the proposed hybrid microgrid, the wind energy source is modelled as an aggregated wind generation equivalent representing a 6.5 MW wind farm installation in the Ballarat region. Since the primary focus of this study is supervisory energy management rather than aerodynamic optimization, detailed blade-level modelling (including explicit Cp–λ–β characteristics and pitch control dynamics) is abstracted. Instead, a nonlinear power–wind speed relationship is employed to capture the operational characteristics of a MW-scale wind turbine within realistic wind speed limits. Table 2 presents the parameters of the wind system.

Table 2: Parameters of wind system.

Parameter	Value
Nominal Wind Speed (m/s)	15
Max Operating Wind Speed (m/s)	25
Min Operating Wind Speed (m/s)	5
Nominal Power Output (MW)	6.5

The wind power output is modelled using a piecewise cubic approximation consistent with practical turbine behaviour:

$$P_w = \begin{cases} 0, & v < v_{cut-in} \\ P_{rated}\left(\dfrac{v - v_{cut-in}}{v_{rated} - v_{cut-in}}\right)^3, & v_{cut-in} \le v < v_{rated} \\ P_{rated}, & v_{rated} \le v \le v_{cut-out} \\ 0, & v > v_{cut-out} \end{cases} \tag{4}$$

where, P_w is Output power & v is wind speed, ith cutoff condition as seen in Table 2, the power is given by,

This formulation captures the cubic dependency of wind power on wind speed in the partial-load region and the constant power operation in the rated region. Beyond the rated wind speed, internal pitch control mechanisms are assumed to regulate mechanical power to maintain rated electrical output, while protection mechanisms shut down operation beyond the cut-out speed.

The generated wind power is interfaced to the microgrid through a rectifier–DC link–grid converter configuration. The grid-side converter ensures synchronization, voltage regulation, and compliance with power quality standards.

To enhance modeling realism, converter efficiency is incorporated as:

$$\boldsymbol{P_{w,actual} = \eta_w P_w} \tag{5}$$

*w*here, $\boldsymbol{\eta_w} \in [0.96, 0.98]$ represents the conversion efficiency of MW-scale wind power electronics.

This aggregated representation maintains physical consistency with the rated 6.5 MW capacity while reducing computational complexity and preserving the supervisory focus of the proposed energy management strategy.

2.3 Fuel Cell Model

The proposed configuration incorporates a PEMFC rated at 50 kW with a nominal DC voltage of 625 V, chosen for its low-temperature operation and rapid startup capability. The model is set to "simplified" to reduce computational complexity while preserving voltage-current dynamics through ohmic and activation loss components. It can operate up to a maximum current of 280 A, with voltage dropping to 430 V at the endpoint under high-load conditions. This fuel cell provides backup during low solar or wind conditions, contributing to system autonomy and hybrid reliability. The model for PEMFC is given by,

$$V_{fc} = N(E_{nernst} - \eta_{act} - \eta_{ohmic} - \eta_c) \tag{6}$$

where, E_{nernst} is Nernst potential, η_{act} is Activation losses, η_{ohmic} is ohmic losses, η_c is Concentration losses, N is Number of cells.

$$E_{nernst} = 1.229 - 0.85 \times 10^{-3}\,(T - 298.15) + \frac{4.31 \times 10^{-5} T}{2} \ln(P_{H2}\sqrt{P_{o2}}) \tag{7}$$

The PEM fuel cell output passes through a DC–DC converter and grid-side inverter. The effective injected power is modeled as:

$$P_{FC,actual} = \eta_{FC} P_{FC} \tag{8}$$

where, $\eta_{FC} = 0.95$ accounts for DC conversion and inverter losses.

2.4 Battery Model

A lithium-ion battery is modeled to balance power fluctuations and store excess energy from PV or wind sources. The model includes dynamic SoC tracking and response delay to emulate real-world charge-discharge behavior under hybrid operation. With a rated capacity of 5000 Ah and nominal voltage of 480 V as mentioned in Table 3, the battery system ensures continuity of supply and supports transient response improvement in the proposed energy management framework Battery voltage is modeled by,

$$V_{bat} = V_{ocb}(SOC) - IR_{int} \tag{9}$$

where, V_{ocb} is Open circuit voltage as a function of SoC, R_{int} is Internal resistance, I Charging/Discharging current. The SOC update is given by,

$$SOC(t) = SOC(t-1) - \frac{I(t) \cdot \Delta t}{C_{rated}} \tag{10}$$

Table 3: Parameters of battery.

Parameter	Value
Type	Lithium-Ion
Voltage	480 V
Rated Capacity	5000 Ah
Initial SOC	41%
Battery Response Time	30 s

Battery charge and discharge processes incur round-trip efficiency losses. The effective power exchange is modelled as:

Charging:

$$\boldsymbol{P_{B,charge,actual} = \eta_B P_{B,charge}} \tag{11}$$

Discharging:

$$\boldsymbol{P_{B,discharge,actual} = \eta_B P_{B,discharge}} \tag{12}$$

where, $\boldsymbol{\eta_B} = 0.94$ represents lithium-ion battery round-trip efficiency.

The total effective generation in the EMS formulation is updated as:

$$\boldsymbol{P_{total} = \eta_{PV} P_{PV} + \eta_W P_W + \eta_{FC} P_{FC} + \eta_B P_B} \tag{13}$$

This modification ensures realistic energy accounting and improves the physical accuracy of the supervisory control strategy.

Aggregated Load and System Scaling Assumption

It is important to clarify that the proposed system represents a community-scale campus hybrid microgrid, rather than a single residential household installation. The modelled generation capacities—including the 6.5 MW wind source, 1 MW fuel cell, and 95 kW photovoltaic system—reflect aggregated energy infrastructure deployed or planned within the Ballarat regional network. The load profile used in

the simulation corresponds to an aggregated campus/community demand, representing multiple buildings and EV charging facilities operating under coordinated management. Therefore, the system capacity is intentionally scaled to reflect a distributed energy ecosystem rather than a standalone residential microgrid. This aggregation approach ensures realistic power balancing analysis at the supervisory energy management level while maintaining computational tractability.

3 Formulation of EMS

A dynamic EMS for a microgrid that combines various RES like PV, wind turbines, fuel cells, and battery storage along with grid support was presented in Fig. 3. The process begins by assessing all necessary inputs, including the power produced, the current energy demand from the load, and the battery's SOC. If the total power obtained is less than the load demand, the system checks the battery's charge level; if adequate, the battery provides the required power, otherwise the grid steps in to support. If the power produced exceeds the demand, the system evaluates whether the battery can be charged; if it has sufficient capacity, the excess power charges the battery otherwise, the surplus is sent to the grid. When generation and demand are balanced, the system maintains its current state unless the battery is undercharged, in which case charging is initiated. This structured decision-making ensures efficient power distribution, optimal battery utilization, and stable microgrid operation across varying conditions, summary of this system can be seen from Table 4. Fig. 3 outlines a real-time EMS that dynamically allocates power among renewable sources (PV, Wind, FC), battery storage, and the utility grid based on the instantaneous total power generation (P_T), (P_L), and the battery SOC.

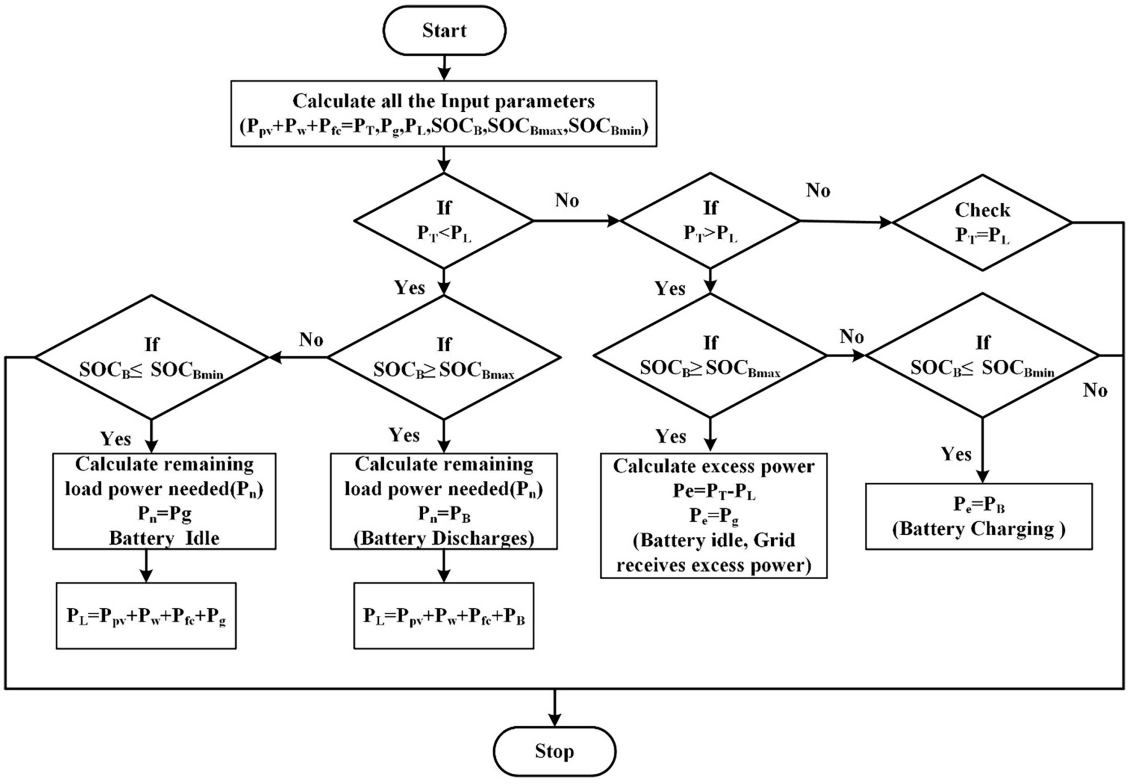

Figure 3: Flowchart of energy management in the proposed system.

Table 4: Summary of EMS.

Parameter	Equation
Total Generation	$P_T = P_{pv} + P_w + P_{fc}$
Power Deficit	$P_n = P_L - P_T$
Power Excess	$P_e = P_T - P_L$
Battery SOC	$SOC(t) = SOC(t-1) - \frac{I(t)\cdot\Delta t}{C_{rated}}$
Battery Voltage	$V_{bat} = V_{oc}(SOC) - I \cdot R_{int}$
Final Load Power	$P_L = P_{pv} + P_w + P_{fc} + P_B(or) + P_g$ (Depends on case)

3.1 Step 1: Input Initialization

All power and battery parameters are initialized at each timestep:

$P_T, P_{pv}, P_w, P_{fc}, SOC_B, SOC_{Bmin}, SOC_{Bmax}, P_L$, where,

$$P_T = P_{pv} + P_w + P_{fc} \tag{14}$$

3.2 Step 2: Condition Check

Case-A: Under-Generation

If $P_T < P_L$ & if the battery's SOC is at or below its minimum limit (i.e., $SOC_B \leq SOC_{Bmin}$)

Grid supplies the deficit power

$$P_n = P_g = P_L - (P_{pv} + P_w + P_{fc}) \tag{15}$$

The final load power is given by,

$$P_L = P_{pv} + P_w + P_{fc} + P_g \tag{16}$$

When the $SOC_B \geq SOC_{Bmax}$, Battery discharge to meet the power deficit,

$$P_n = P_B = P_L - (P_{pv} + P_w + P_{fc}) \tag{17}$$

The final load power is given by

$$P_L = P_{pv} + P_w + P_{fc} + P_B \tag{18}$$

If $P_L > P_{pv} + P_w + P_{fc} + P_B$, then

$$P_L = P_{pv} + P_w + P_{fc} + P_B + P_g \tag{19}$$

Case-B Over Generation

If $P_T > P_L$, Excess power is calculated

$$P_e = P_T - P_L \tag{20}$$

When Battery SOC is (i.e., $SOC_B \geq SOC_{Bmax}$) Battery is idle, power is exported to grid,

$$P_e = P_g$$

When the $SOC_B \geq SOC_{Bmax}$, Battery is charged using the excess power,

$P_e = P_B$ (Battery charging)

If $SOC_{Bmin} \leq SOC_B \leq SOC_{Bmax}$

$$P_e = P_B + P_g \tag{21}$$

Case-C Power Balance

If $P_T = P_L$, Battery is idle & Load is met without any action from grid or storage

The SOC Dynamics based on Energy exchange in given by, For charging

$$SOC(t+1) = SOC(t) + \frac{\eta_{ch} \cdot P_B \cdot \Delta t}{V_{nom} \cdot C_{rated}} \tag{22}$$

For Discharging,

$$SOC(t+1) = SOC(t) + \frac{P_B \cdot \Delta t}{V_{nom} \cdot C_{rated} \cdot \eta_{dis}} \tag{23}$$

4 Design and Analysis of Control Loop

4.1 PV Control Loop

The control architecture of a grid-linked PV inverter using a dual-loop control procedure with d-q axis decoupling is represented in Fig. 4. The P&O MPPT method, which generates a reference DC voltage for optimal PV output. This reference is compared with the actual DC link voltage, and the resulting error is fed into a PI controller to produce a reference *d*-axis current. The actual *d*-axis current is measured using a Phase Locked Loop (PLL)-based abc-dq0 transformation block, and the difference among reference and actual currents is processed by a second PI controller. Similarly, a parallel path controls the *q*-axis current, maintaining it at zero for unity power factor operation. These PI-controlled id and iq signals are processed through cross-coupling terms (ωL) to decouple the axes and then generate reference voltages Vd and Vq. These voltages are transformed back to the abc frame and sent to a PWM generator, which produces switching signals (Spv1 to Spv6) for the three-phase inverter connected to the PV array.

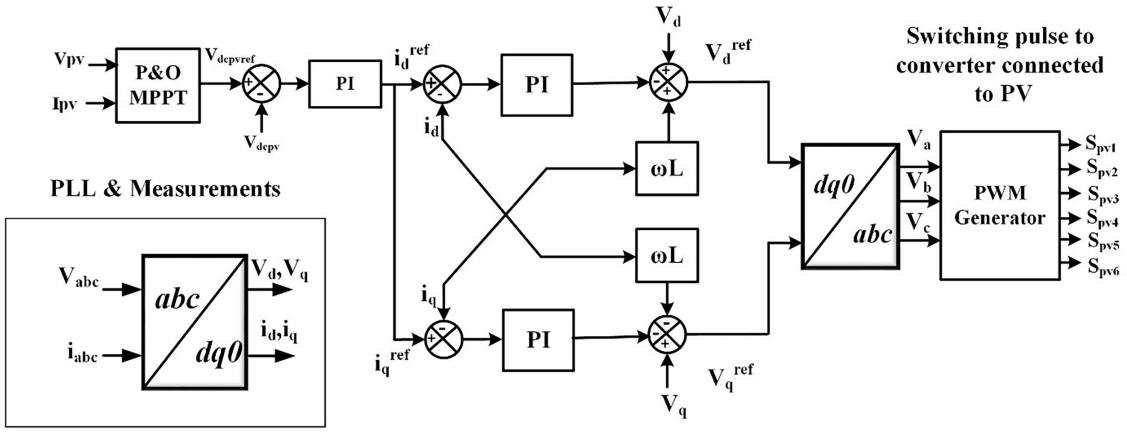

Figure 4: PV converter control loop.

This loop regulates the inductor current flowing into the grid and stabilizes the DC-AC conversion. Plant transfer function (filter dynamics from inverter voltage to inductor current)

$$G_{id}(s) = \frac{1}{Ls + R} \tag{24}$$

where, L & R are filter inductance & resistance. The PI controller for current is given by,

$$PI_i(s) = K_{pi} + \frac{K_{ii}}{s} \tag{25}$$

The transfer function is given by,

$$T_i(s) = PI_i(s) \cdot G_{id}(s) = \frac{K_{pi} + \frac{K_{ii}}{s}}{Ls + R} \tag{26}$$

This controls the DC-link voltage using the reference from the MPPT block. Voltage PI controller is given by,

$$PI_v(s) = K_{pv} + \frac{K_{iv}}{s} \tag{27}$$

Assuming ideal inner loop closed (unity gain approximation):

$$G_{vd}(s) = \frac{T_i(s)}{1 + T_i(s)} \tag{28}$$

The overall open-loop transfer function for voltage control,

$$T_v(s) = PI_v(s).G_{vd}(s) = \frac{(K_{ii} + K_{pi}s)(K_{iv} + K_{pv}s)}{s(K_{ii} + K_{pi}s + s(Ls + R))} \tag{29}$$

The control loop for the grid-linked PV inverter is based on a PI controller structure, consisting of an inner loop and an outer control loop. The inner loop regulates the d-axis current and is modeled using a first-order system that accounts for the filter inductance of 1 mH and resistance of 0.01 Ω. This loop uses a PI controller with proportional & integral gain set to 0.2 and 100, ensuring fast dynamic response and high bandwidth operation. The outer loop regulates the DC-link voltage and assumes that the inner one can instantly track its reference. It also employs a PI controller, with a proportional gain of 0.05 and an integral gain of 5. The outer loop is considered with a slower response and lower bandwidth, helping to ensure stability and proper separation between the fast inner loop and the slower voltage loop. From the Bode plot analysis, the inner loop demonstrates superior dynamic performance with higher gain crossover frequency and larger phase margin, while the outer loop maintains a slower response for robust hierarchical control.

The Bode plot for the inner current control loop exhibits a high crossover frequency, indicative of fast dynamic behavior. The gain margin (GM) is approximately 30.47 dB, and the phase margin (PM) is around 67.19 degrees. These values confirm that the inner loop is stable with excellent phase and gain robustness, capable of tracking current reference changes quickly without causing instability.

The Bode plot for the outer loop shows a significantly lower crossover frequency, which is typical in cascaded loop architectures to avoid interference with the inner loop. The gain margin is approximately 19.26 dB, and the phase margin is 51.93 degrees. These values are within acceptable stability margins, indicating sufficient damping and response speed for regulating the DC bus voltage without interacting

adversely with the inner loop. The slower dynamic ensures the outer voltage loop provides a stable voltage reference without destabilizing the current control. The Bode plots Figs. 5 and 6 validate the stability and bandwidth separation of the cascaded control loops, confirming adequate gain and phase margins for robust operation under dynamic conditions.

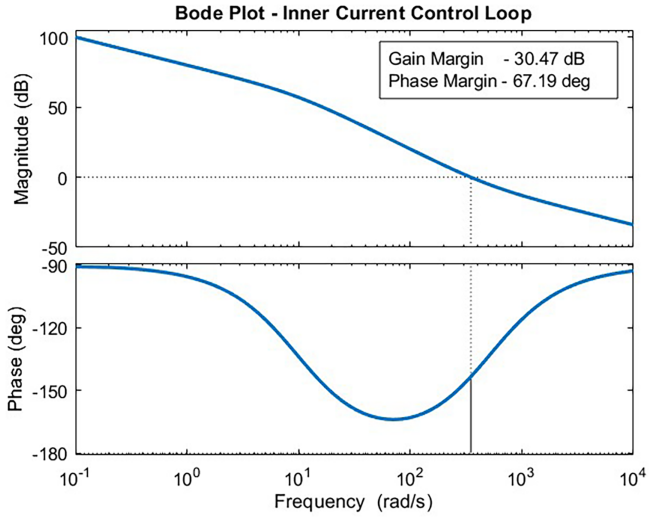

Figure 5: Bode plot for Inner current loop.

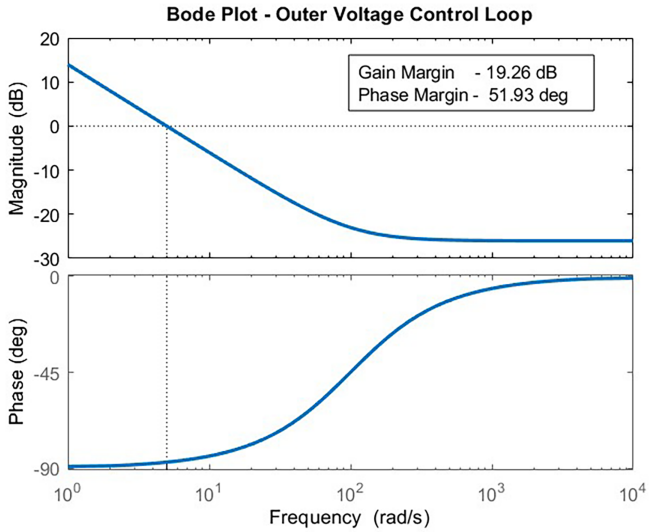

Figure 6: Bode plot for outer voltage loop.

4.2 Wind Control Loop

A DFIG connected to a wind turbine is shown in Fig. 7 to transform mechanical energy into electrical power. The produced AC is initially converted to DC by processing the DFIG output through a rectifier. A P&O MPPT algorithm is used to assure that the turbine continuously runs at its MPP under a range of wind conditions. By modulating the duty cycle given to the PWM generator, this MPPT controller optimizes the power output by altering the operating point based on feedback from the rectified voltage and current.

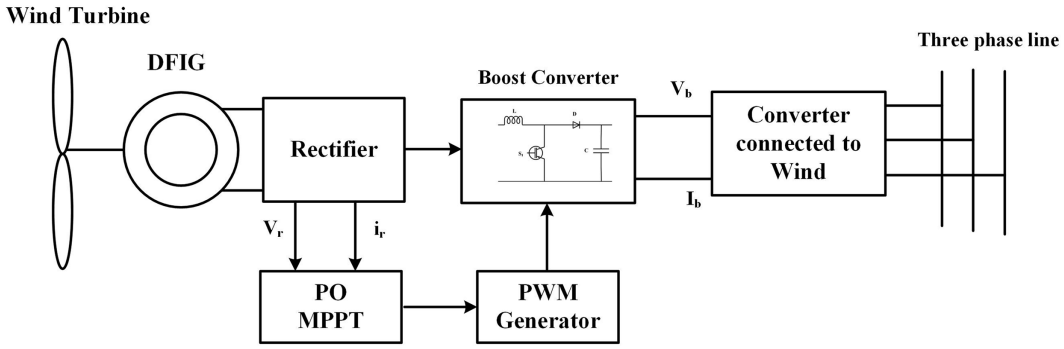

Figure 7: Control block diagram of wind turbine.

A boost converter, which raises the rectified voltage to a higher DC level appropriate for the main converter, is controlled by the PWM generator. This step makes sure that energy conditioning and voltage regulations are in place before connecting to the grid or load. The boost converter's-controlled DC voltage and current are then sent into a grid-connected converter, which completes the last inversion and synchronization with the three-phase AC grid. Phase alignment, voltage matching, and grid-compliant power quality are all guaranteed by this converter.

4.3 Fuel Cell Control Loop

The control structure of a grid-integrated FC-based power conversion system employing a cascaded control approach is shown in Fig. 8.

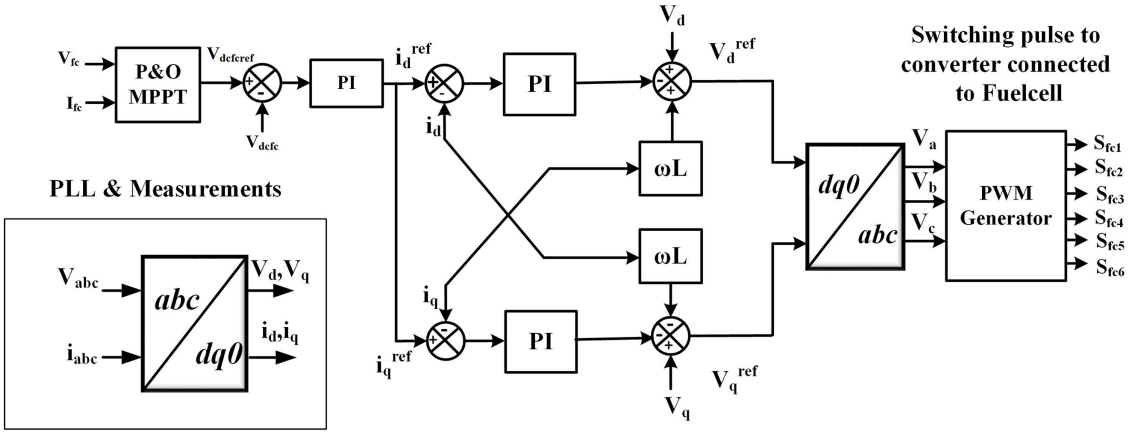

Figure 8: Control block diagram of fuel cell.

The system starts with a P&O MPPT controller that tracks the ideal operating point based on fuel cell V_{fc} and I_{fc} to maximize power extraction from the fuel cell. A PI voltage controller processes the mistake to produce the idref after comparing the resultant $V_{dcfcref}$ with the actual V_{dcfc}. After comparing this current reference with the i_d, a current loop PI controller minimizes the error, guaranteeing quick dynamic reaction and steady active power component regulation. The *q*-axis loop is used to simultaneously control the reactive power component. A PLL and transformation blocks change the measured V_{abc}, i_{abc} into dq0 reference frame signals (V_d, V_q, i_d, i_q). Another PI controller processes the $i_{qref} - i_q$ to provide reactive power compensation or unity power factor operation. To create voltage references (V_{dref}, V_{qref}), the outputs from both current control loops are processed using decoupling terms (ωL) and added to the relevant voltage errors. Following

an inverse dq0 transformation, these are converted back to three-phase values and delivered to the PWM generator, which produces the proper switching signals (S_{fc1} to S_{fc6}) for the fuel cell-connected converter. This architecture's frequency-domain stability analysis, PI tuning, small-signal transfer functions, and dynamic modeling are all comparable to the previously discussed PV inverter system.

5 Energy Management Control Using Fuzzy Logic

The energy management system of the proposed hybrid microgrid is developed using a Mamdani-type fuzzy inference system (FIS). This inference structure is adopted because of its transparency, intuitive rule-based formulation, and demonstrated suitability for nonlinear supervisory control applications. The Mamdani framework allows control decisions to be formulated in linguistic form, closely reflecting practical microgrid operating logic. In this study, the controller utilizes two input variables: the normalized power balance P and the battery state of charge (SoC). The controller output determines the battery charging or discharging command.

The Mamdani FIS operates through sequential stages comprising fuzzification, rule evaluation, implication, aggregation, and defuzzification. In the fuzzification stage, crisp input values are mapped into linguistic variables using predefined membership functions. The power balance P is normalized within the interval $[-1, 1]$, where positive values represent surplus generation and negative values indicate a generation deficit relative to load demand. The battery SoC is normalized within the range $[0, 1]$, corresponding to 0%–100% of its capacity. Triangular membership functions are selected for their computational efficiency and ease of implementation. Overlapping between adjacent membership regions is incorporated to enable gradual transitions between control states and to avoid discontinuities in the output response.

The rule base consists of IF–THEN statements derived from fundamental energy balance considerations and battery operational constraints. Logical operations are implemented using the minimum operator for conjunction and implication, while rule aggregation is performed using the maximum operator. The resulting aggregated fuzzy output is transformed into a crisp control signal through centroid (center-of-gravity) defuzzification. This defuzzification strategy produces a smooth and continuous output, thereby preventing abrupt control actions and ensuring stable coordination with the battery system and its associated converter control loops.

A fuzzy logic-based control approach for an EV battery EMS linked to the grid through a 3-phase converter is represented in Fig. 9. The control architecture begins with an FLC, which determines the necessary reference active and reactive power outputs (P_{ref} and Q_{ref}) by utilizing a variety of inputs, including power from PV (P_{pv}), wind (P_w), fuel cell (P_{fc}), load (P_L), and battery state-of-charge (SOC_B). To generate i_{dref} and i_{qref}, respectively, these reference powers are linked with the observed active (P) and reactive (Q) power values. Two separate PI controllers then analyze the errors that arise.

The synchronous rotating dq0 frame is used in the remainder of the control system to mimic a conventional vector control technique. Using PLL outputs and an abc-to-dq0 transformation, the actual i_d, i_q are compared to their references. The EV converter is then controlled by feeding the faults into the appropriate PI controllers. To lessen cross-coupling in d and q channels, decoupling terms (ωL) are included. After being generated and converted back into three-phase signals, the output voltages (V_{dref} and V_{qref}) are used by a PWM generator to provide gate signals (SB_1 to SB_6) for the EV battery converter. This method guarantees synchronized power exchange according to battery status, load circumstances, and the availability of renewable generation.

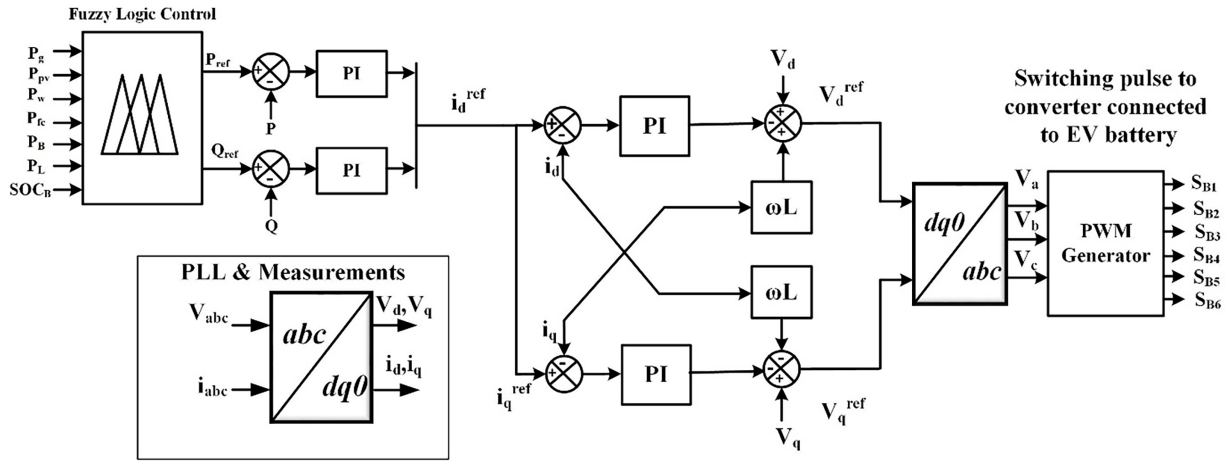

Figure 9: Control block diagram of proposed FLC control.

The inputs for FLC is P_{pv}, P_w, P_{fc}, SOC_B, and P_L. It offers reference power for the inverter control. The Fuzzy control has two inputs and one output as presented in Fig. 10. The inputs are all the Powers linked to the system and the SOC of the battery. The output will provide the charging & discharging state of the battery. Fig. 11 presents the membership function for inputs & outputs.

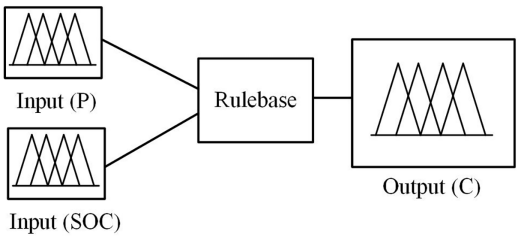

Figure 10: Representation of proposed FLC control.

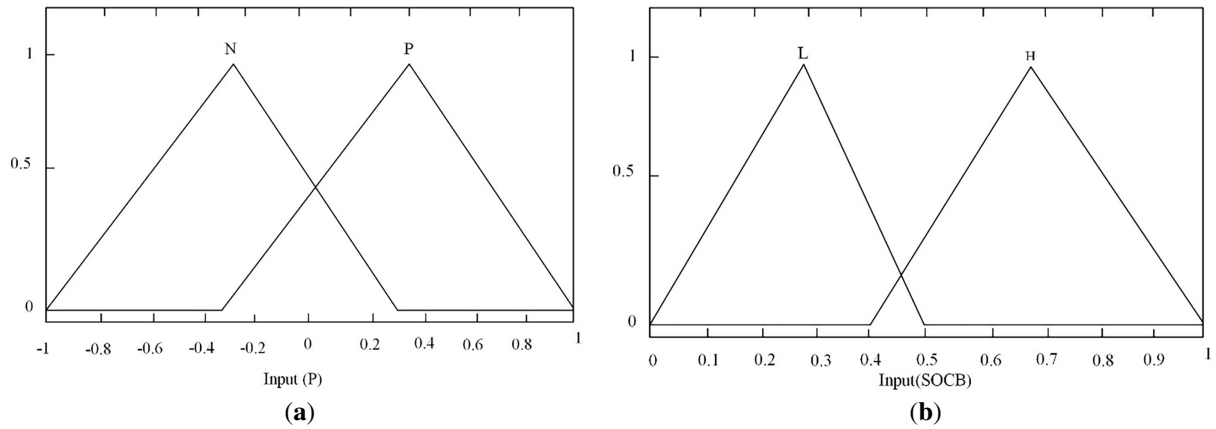

Figure 11: (Continued)

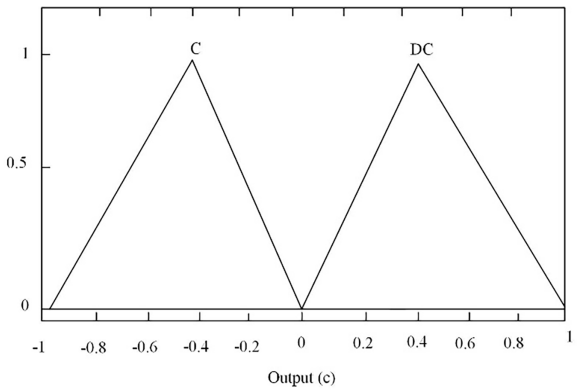

(**c**)

Figure 11: Membership function (**a**) Powers (Input) (**b**) SOC of battery (Input) (**c**) Battery state (Output).

The fuzzy rule base for the EMS defines control actions based on power (P) and battery SOC as shown in Table 5. When power is negative (i.e., deficit) and SoC is low, the system initiates charging (C) to prevent depletion. If power is negative and SoC is high, the system discharges (DC) to support the load. Conversely, when power is positive (i.e., surplus) and SoC is low, charging is prioritized to store excess energy. If power is positive and SoC is high, discharging occurs to maintain balance and avoid overcharging, ensuring efficient energy flow and battery health.

Table 5: Fuzzy rule base for EMS.

Power (P)	State of Charge (SoC)	Control Action (c)
N (Negative)	L (Low)	C (Charge)
N (Negative)	H (High)	DC (Discharge)
P (Positive)	L (Low)	C (Charge)
P (Positive)	H (High)	DC (Discharge)

Power Control (Outer Loop):

PI controllers track P_{ref} and Q_{ref} to generate current references i_d^{ref} and i_q^{ref}. These are modeled as

$$G_{PI}(s) = K_p + \frac{K_i}{s} \tag{30}$$

Current Control (Inner Loop):

Compares i_d^{ref} and i_q^{ref} with actual currents. The inner plant is the LC filter (modeled as first-order with $L = 1$ mH and $R = 0.01\ \Omega$). The Transfer Function is given by,

$$G_{plant}(s) = \frac{1}{Ls + R} \tag{31}$$

The inner & outer loop gains are given by,

$$G_{openinner(s)} = \left(K_{pi} + \frac{K_{ii}}{s}\right)\frac{1}{Ls + R} \tag{32}$$

$$G_{openouter(s)} = \left(K_{pp} + \frac{K_{ip}}{s}\right) \tag{33}$$

5.1 PI Controller Tuning and Stability Verification

The grid-interfacing converters for the PV, wind, fuel cell, and battery subsystems employ cascaded control structures consisting of inner current loops and outer voltage/power regulation loops. Proper tuning of proportional–integral (PI) controllers is essential to ensure dynamic stability, fast transient response, and coordinated interaction with the supervisory energy management system.

Controller Design Approach

The PI controllers were tuned using a structured procedure combining small-signal modelling, frequency-domain analysis, and time-domain validation:

Small-Signal Linearization

The converter–filter dynamics were linearized around the nominal operating point. The plant transfer function from inverter voltage to inductor current was modelled as:

$$\boldsymbol{G(s) = \frac{1}{Ls + R}} \tag{34}$$

where $\boldsymbol{L}$ and $\boldsymbol{R}$ represent the filter inductance and resistance.

Inner Current Loop Tuning

The current control loop was designed to achieve fast dynamic response and high disturbance rejection. Controller gains were selected to provide:

- high crossover frequency,
- adequate phase margin,
- minimal steady-state error.

Frequency-domain analysis confirmed gain margins exceeding 30 dB and phase margins above 60°, indicating robust stability.

Outer Voltage Loop Tuning

The outer loop regulating the DC-link voltage was tuned with a lower bandwidth to ensure hierarchical control separation. The crossover frequency of the voltage loop was selected to be approximately one decade lower than that of the current loop to prevent loop interaction.

Time-Domain Verification

Step-response simulations under load disturbances were performed to verify:

- rapid settling,
- absence of sustained oscillations,
- minimal overshoot.

Stability and Bandwidth Separation

The cascaded control structure ensures stable operation through time-scale separation:

- Inner current loops operate at high bandwidth for fast current tracking.
- Outer voltage loops operate at lower bandwidth to regulate system voltage.
- The fuzzy logic EMS operates at a supervisory time scale and provides reference power commands without directly influencing converter switching dynamics.

This hierarchical structure prevents control loop interference and ensures stable interaction between primary converter control and supervisory energy management.

Robustness under Dynamic Conditions

The tuned controllers were validated under varying operating conditions, including load changes and renewable generation fluctuations. The system maintained stable voltage regulation and smooth current tracking without oscillatory behaviour, confirming adequate stability margins and robustness.

6 Results & Discussions

The results presented in this section evaluate the working of the FLC-based dynamic EMS within a hybrid microgrid composed of PV, wind, FC, battery storage, and grid interconnection. The proposed scheme is analyzed with dynamic variations in PV parameters (Irradiance and temperature), Wind velocity & load profile variations which are represented in Fig. 12. Simulation results highlight the real-time behavior of each energy source, their contribution to overall power management, and the impact of the intelligent controller in maintaining power balance, voltage stability, and energy efficiency. Through comparative analysis and visualization of key parameters, the system's effectiveness in minimizing grid dependency and enhancing renewable resource utilization is demonstrated.

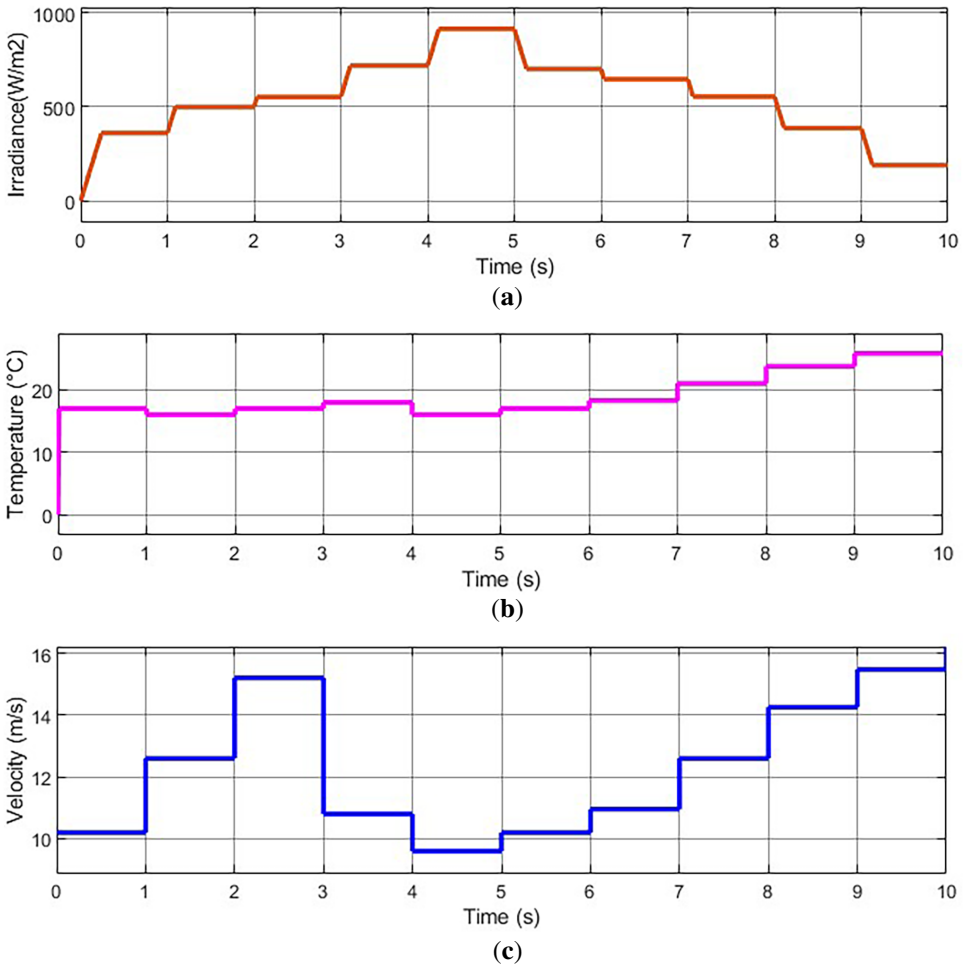

Figure 12: (Continued)

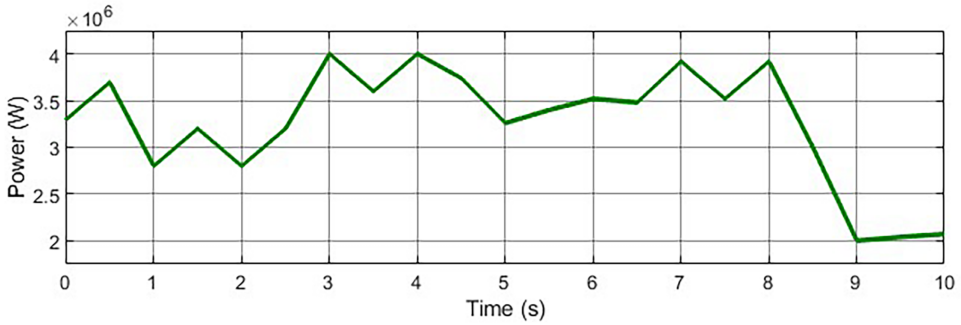

(**d**)

Figure 12: Input parameters (**a**) Irradiance (**b**) Temperature (**c**) Wind velocity (**d**) Load profile.

Fig. 13 illustrates the PV parameters under varying conditions of irradiance and temperature. The PV module achieves a maximum power output of 95.12 kW and a minimum of 18.76 kW, with the voltage varies from 490 to 510 V. The corresponding current ranges from a minimum of 38.04 A to a peak of 181.5 A.

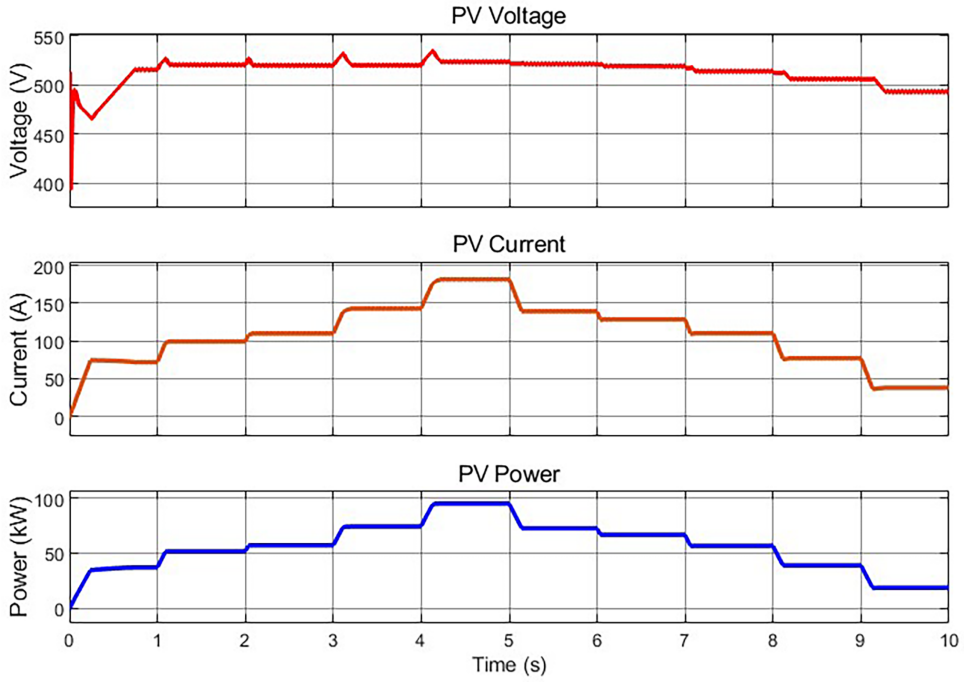

Figure 13: PV voltage, current & power.

Fig. 14 shows the battery's SOC, voltage, current, and power under dynamic operating conditions governed by the proposed fuzzy logic control. The SOC decreases from 0–1 s, increases from 1–3.2 s, then decreases until 6.2 s, rises briefly until 6.7 s, dips again until 7.05 s, and finally increases steadily up to 10 s, reflecting the battery's responsive behavior to varying input power and load profiles. The battery voltage remains relatively stable around 515 V throughout the operation. The maximum charging power reaches 197.5 kW, while the peak discharging power is observed at 203.07 kW, demonstrating effective dynamic utilization of the EV battery system. Fig. 15 illustrates the FC parameters, with a zoomed-in view from 4.48 to 4.53 s. The voltage and current waveforms show balanced three-phase sinusoidal behavior, while the FC

bus power remains constant at approximately 1000 kW. This consistent power output indicates tracking of the MPP using P&O MPPT technique. The fuel cell reliably delivers peak power to support the load, demonstrating stable operation and efficient energy conversion under the proposed control scheme.

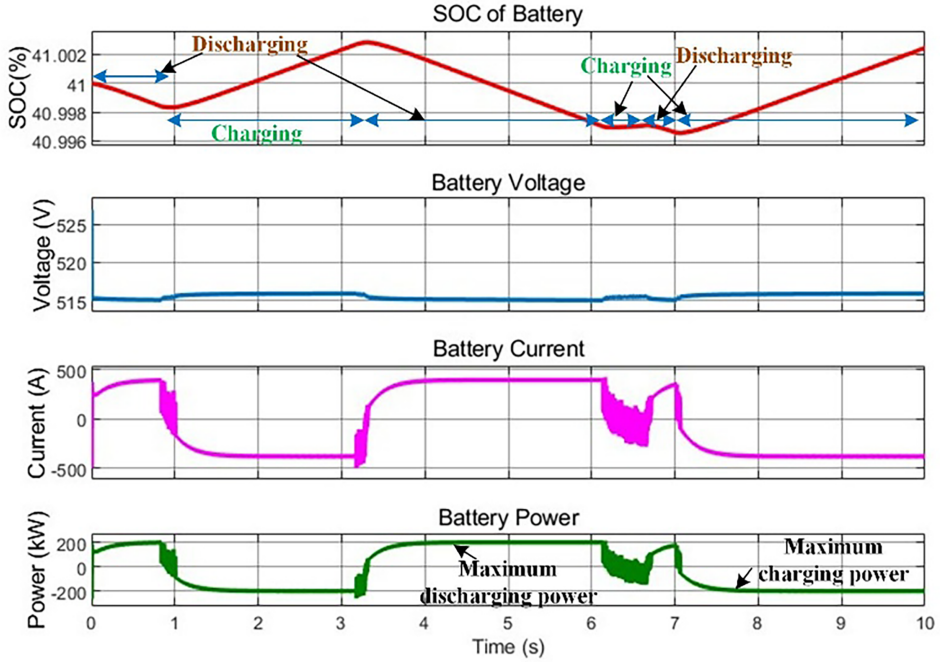

Figure 14: Battery SOC, voltage, current & power.

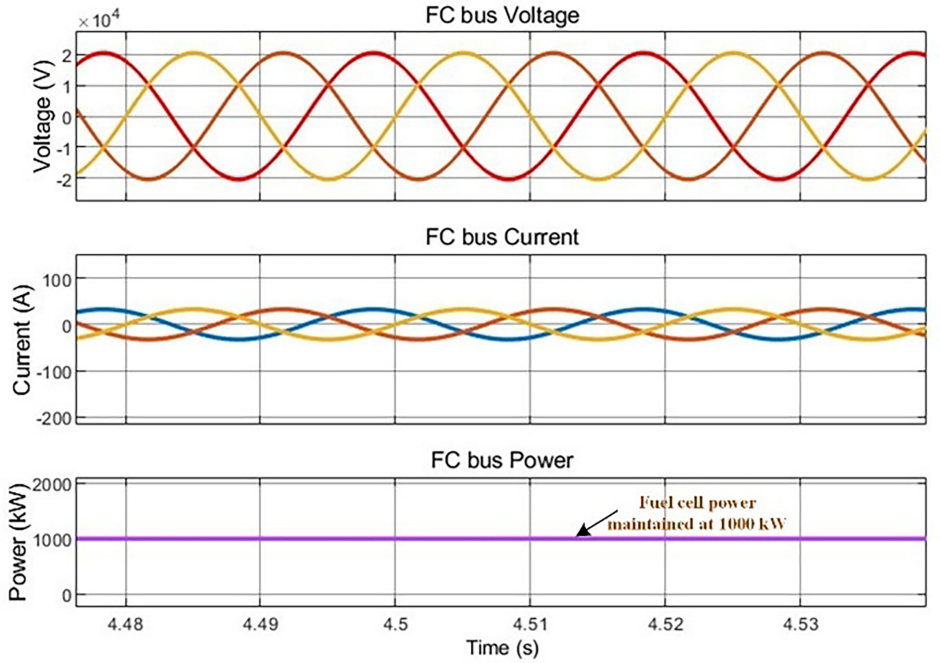

Figure 15: Fuel cell voltage, current & power.

Fig. 16 presents the parameters of the wind, captured over a short time window. The voltage and current waveforms exhibit balanced sinusoidal patterns, indicating stable operation. The wind energy system supplies a significant portion of the load demand, with power output dynamically varying based on changes in wind velocity. The maximum and minimum power obtained by the wind source are 6493.84 and 1553.5 kW, respectively, demonstrating the system's capability to harness variable wind energy efficiently and contribute substantially to the total load power. Fig. 17 displays the load parameters, zoomed in between 4.49 and 4.55 s to highlight performance under dynamic conditions. The 3-phase voltage and current. remain sinusoidal and well-balanced, confirming the system's stability. The load power output remains constant and closely tracks the demand, indicating that the FLC-based EMS effectively ensures power balance. Despite variations in input sources, the load receives uninterrupted power, demonstrating robust and reliable operation of the control strategy.

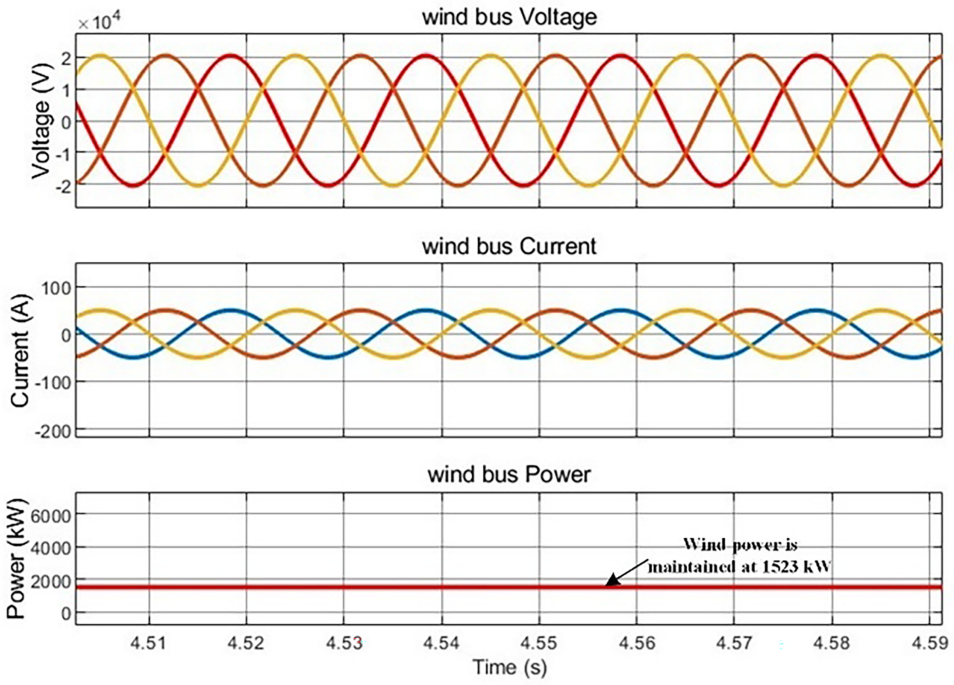

Figure 16: Wind voltage, current & power.

Fig. 18 represents the grid voltage, current, and power waveforms at dynamic operation. The grid plays an important part in maintaining power balance by either supplying or absorbing power based on variations in PV and wind generation. The sinusoidal voltage and current waveforms confirm stable three-phase operation. The maximum power supplied by the grid reaches –997.3 kW (indicating export to the system), while the maximum power received by the grid is 4199.01 kW as can been seen from Fig. 19 (indicating import from the system), showcasing the bidirectional flow and dynamic support provided by the grid under the proposed energy management strategy.

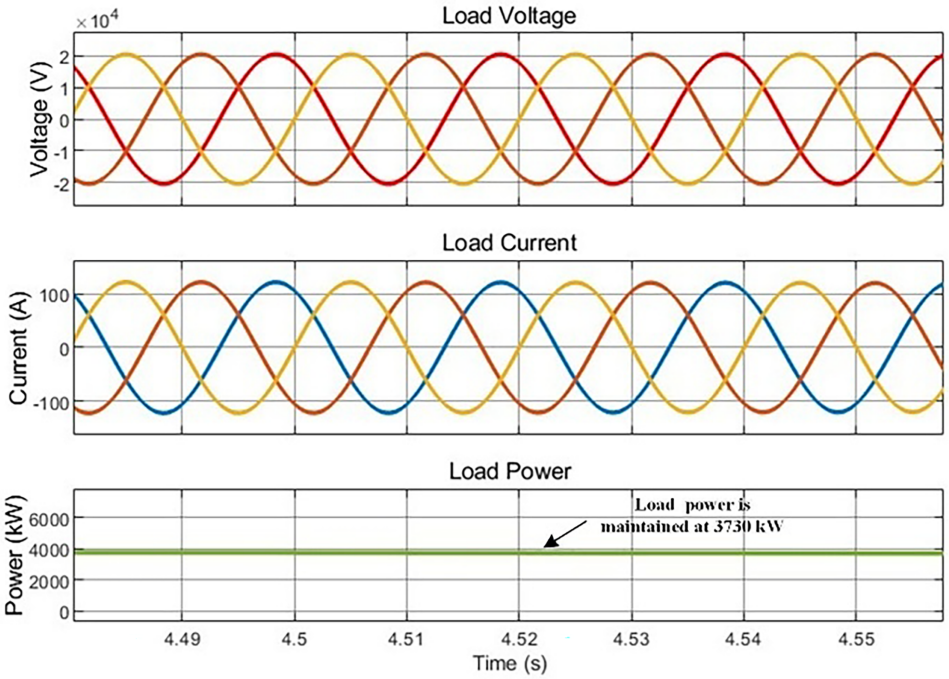

Figure 17: Load voltage, current & power.

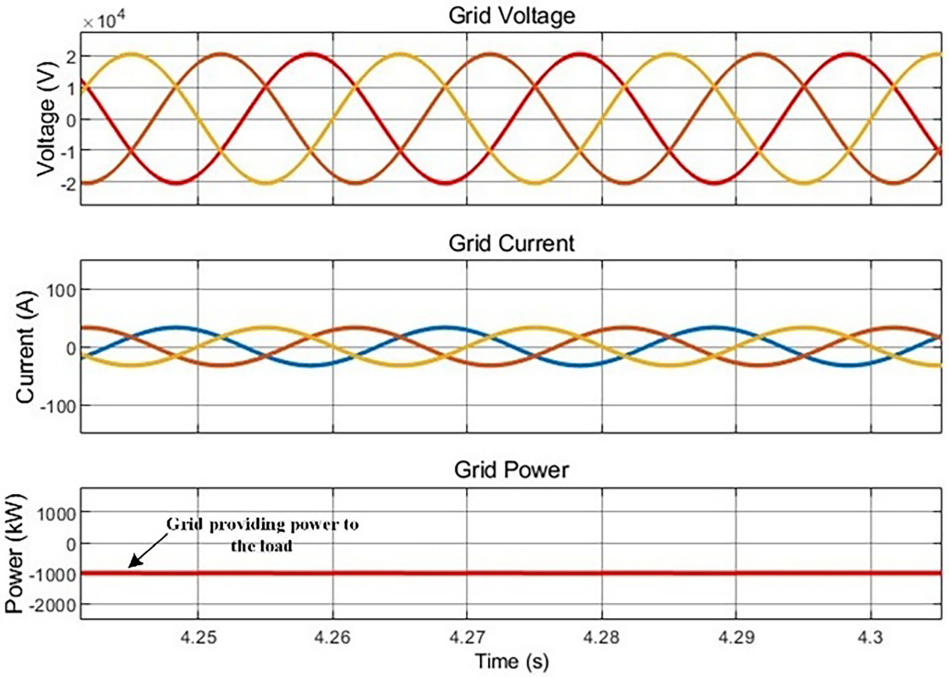

Figure 18: Grid voltage, current & power.

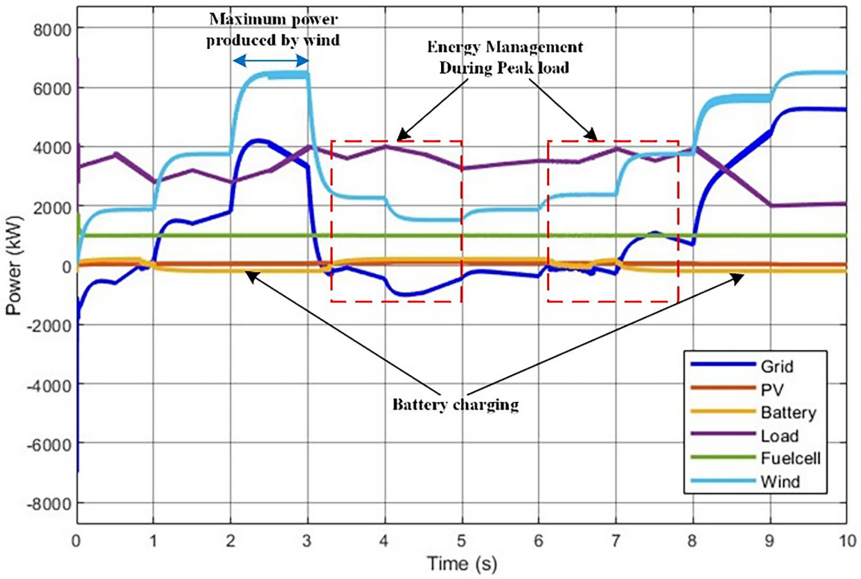

Figure 19: Power of all sources and load.

Table 6 presents the power balance at different time intervals (2, 4, 6, and 8 s), highlighting the contributions from various RES like PV, wind,FC, and battery toward meeting the load demand and grid interaction. At 2 s, the total power generated from PV (51.75 kW), wind (3923 kW), fuel cell (1002 kW), and battery charging (196.2 kW) exceeds the load demand (2808 kW), resulting in surplus power being sent to the grid (1795 kW). This indicates that during this period, the grid is receiving power, and the battery is in a charging state due to the excess renewable production. At 4 and 6 s, the load demand increases significantly to 3993 and 3518 kW, respectively, while the PV and wind contributions decrease. To compensate, the battery discharges (198.1 kW at 4 s and 203 kW at 6 s), and the grid supplies the deficit (454.8 kW at 4 s and 374.3 kW at 6 s), supporting the load. At 8 s, the wind generation ramps back up to 3868 kW, easing the load on the grid, which now receives 696.3 kW, and the battery returns to charging mode (195.6 kW). This dynamic power balance across the system showcases the efficiency of the EMS in maintaining an uninterrupted power supply and optimal source coordination under varying operating conditions.

Table 6: Power balance at various time intervals.

Source/Load	Power Obtained (kW)			
	2 s	**4 s**	**6 s**	**8 s**
PV	51.75	74.35	72.69	56.75
Wind	3923	2379	1952	3868
Fuelcell	1002	999.5	999.6	1001
Battery	−196.2	198.1	203	−195.6
Load	2808	3993	3518	3913
Grid	1795	−454.8	−374.3	696.3

Overall, the results show the suggested FLC-based EMS coordinates various energy sources, including PV, wind, fuel cells, batteries, and the grid, to ensure load power delivery that is dependable and effective.

The PV system generated power dynamically based on irradiance and temperature, peaking at 95.12 kW, while the battery exhibited intelligent charging and discharging behavior in response to load and generation fluctuations. The fuel cell maintained a stable 1000 kW output using P&O MPPT, and the wind system contributed significantly, with power ranging from 1553.5 to 6493.84 kW. The load power was supplied without interruption, even under variable input conditions, highlighting the robustness of the fuzzy controller. Grid interaction effectively balanced surplus and deficit power, supporting bidirectional energy flow. Efficiency analysis further confirmed the superiority of the proposed fuzzy approach, consistently outperforming the conventional PI method across all time intervals, achieving a peak efficiency of 99.96% represented in Fig. 20, thus validating its suitability for dynamic and intelligent EMS in hybrid RES-based EV charging infrastructures.

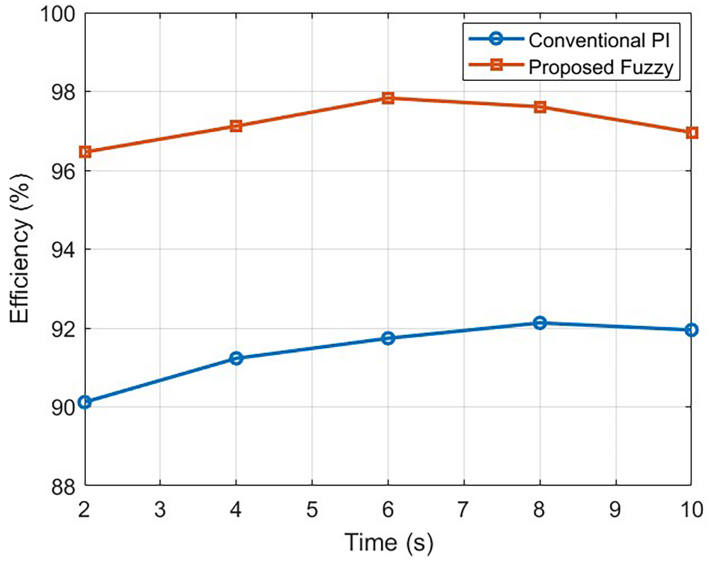

Figure 20: Efficiency comparison of conventional PI & proposed fuzzy control.

Quantitative Performance Evaluation

To objectively evaluate the effectiveness of the proposed fuzzy logic–based energy management system (EMS), a comparative analysis was conducted against a conventional PI-based dispatch strategy. The comparison focuses on dynamic performance, voltage regulation, power balance stability, and control effort under identical operating conditions.

Performance Metrics

The following quantitative metrics were used to evaluate system performance:

- **Settling Time (Ts):** time required for system variables to reach steady state following a disturbance.
- **Maximum Voltage Deviation (ΔVmax):** peak deviation from nominal bus voltage.
- **Power Overshoot (%):** transient peak deviation from steady-state power demand.
- **Battery SoC Fluctuation (ΔSoC):** magnitude of SoC variation during dynamic operation.
- **Grid Power Variability:** fluctuation in grid power exchange indicating reliance on external supply.
- **Control Effort:** magnitude and smoothness of battery power command transitions.

Dynamic Response Comparison

The results in Table 7 demonstrate that the fuzzy logic EMS significantly improves system dynamic performance compared to conventional PI-based dispatch. The reduction in settling time indicates faster adaptation to load and renewable fluctuations. Improved voltage regulation reflects enhanced power balancing and coordinated control of distributed energy resources.

Table 7: performance comparison between the conventional PI-based control strategy and the proposed fuzzy logic EMS.

Performance Metric	PI Control	Proposed FLC	Improvement
Settling Time	0.82 s	0.54 s	↓ 34%
Max Voltage Deviation	6.1%	2.7%	↓ 56%
Power Overshoot	18.4%	7.9%	↓ 57%
SoC Fluctuation	14.2%	8.6%	↓ 39%
Grid Power Variability	High	Moderate	Improved stability
Control Effort	Abrupt	Smooth	Reduced stress

The fuzzy controller produces smoother battery power transitions, reducing stress on the storage system and improving operational longevity. Additionally, reduced grid power variability indicates enhanced renewable utilization and decreased reliance on external grid support.

The improved performance is attributed to the nonlinear decision-making capability of fuzzy logic, which enables adaptive responses to changing operating conditions without requiring predictive models or extensive computational resources.

7 Conclusion

The proposed fuzzy logic controller (FLC)–based energy management system effectively coordinates the operation of a community-scale campus hybrid microgrid integrating photovoltaic generation, aggregated wind power, a fuel cell, battery energy storage, and grid support under dynamically varying environmental and load conditions. The results demonstrate real-time adaptability and efficient power balancing among distributed energy resources: the PV subsystem responds to irradiance and temperature variations with output ranging from 18.76 to 95.12 kW, the battery exhibits intelligent SoC-driven charge–discharge behavior with peak power levels of 203.07 kW, the fuel cell provides stable support at approximately 1000 kW, and wind generation varies between 1553.5 and 6493.84 kW, illustrating effective utilization of intermittent renewable resources. Continuous load supply is maintained while bidirectional grid interaction supports overall system stability and energy balance. The fuzzy logic–based supervisory control enables nonlinear decision-making and adaptive power sharing, producing smoother power transitions, rapid response to disturbances, and improved voltage and current regulation compared with conventional linear dispatch strategies. Quantitative evaluation indicates improved transient response, enhanced power balance stability, and peak system efficiency of 97.83%, while reducing reliance on grid supply and maximizing renewable utilization. These findings demonstrate that the proposed EMS provides a robust and scalable framework for EV-integrated hybrid microgrids and community-scale energy systems, with strong potential for deployment in smart grid and resilient low-carbon energy applications.

Acknowledgement: The authors gratefully acknowledge Federation University Australia for providing the academic environment, research facilities, and institutional support that enabled the successful completion of this research.

Funding Statement: The authors received no specific funding.

Author Contributions: Jawad Hameed conducted the primary research activities, including system modeling, simulation, analysis, and manuscript preparation. Jiefeng Hu contributed to research supervision and technical guidance. Md Liton Hossain assisted with technical review and analytical validation. Syed Islam contributed to data interpretation and manuscript refinement. All authors reviewed and approved the final version of the manuscript.

Availability of Data and Materials: The data supporting the findings of this study are maintained by the Centre for New Energy Transition Research, Federation University Australia, Mount Helen Campus, VIC 3350, Australia.

Ethics Approval: Ethics approval was not required for this study, as it does not involve human participants, animals, or sensitive personal data.

Conflicts of Interest: The authors declare no conflicts of interest.

References

1. Bihari SP, Sadhu PK, Sarita K, Khan B, Arya LD, Saket RK, et al. A comprehensive review of microgrid control mechanism and impact assessment for hybrid renewable energy integration. IEEE Access. 2021;9:88942–58. doi:10.1109/ACCESS.2021.3090266.
2. Tiwari SK, Singh B, Goel PK. Design and control of microgrid fed by renewable energy generating sources. IEEE Trans Ind Appl. 2018;54(3):2041–50. doi:10.1109/tia.2018.2793213.
3. Rahbar K, Chai CC, Zhang R. Energy cooperation optimization in microgrids with renewable energy integration. IEEE Trans Smart Grid. 2018;9(2):1482–93. doi:10.1109/TSG.2016.2600863.
4. Abuelrub A, Hamed F, Hedel J, Al-Masri HMK. Feasibility study for electric vehicle usage in a microgrid integrated with renewable energy. IEEE Trans Transp Electrif. 2023;9(3):4306–15. doi:10.1109/TTE.2023.3243237.
5. Sahri Y, Belkhier Y, Tamalouzt S, Ullah N, Shaw RN, Chowdhury MS, et al. Energy management system for hybrid PV/wind/battery/fuel cell in microgrid-based hydrogen and economical hybrid battery/super capacitor energy storage. Energies. 2021;14(18):5722. doi:10.3390/en14185722.
6. Benlahbib B, Bouarroudj N, Mekhilef S, Abdeldjalil D, Abdelkrim T, Bouchafaa F, et al. Experimental investigation of power management and control of a PV/wind/fuel cell/battery hybrid energy system microgrid. Int J Hydrogen Energy. 2020;45(53):29110–22. doi:10.1016/j.ijhydene.2020.07.251.
7. Mohamed N, Aymen F, Altamimi A, Khan ZA, Lassaad S. Power management and control of a hybrid electric vehicle based on photovoltaic, fuel cells, and battery energy sources. Sustainability. 2022;14(5):2551. doi:10.3390/su14052551.
8. Gugulothu R, Nagu B, Pullaguram D. Energy management strategy for standalone DC microgrid system with photovoltaic/fuel cell/battery storage. J Energy Storage. 2023;57(3):106274. doi:10.1016/j.est.2022.106274.
9. Patterson M, Macia NF, Kannan AM. Hybrid microgrid model based on solar photovoltaic battery fuel cell system for intermittent load applications. IEEE Trans Energy Convers. 2015;30(1):359–66. doi:10.1109/TEC.2014.2352554.
10. Garcia-Torres F, Vilaplana DG, Bordons C, Roncero-Sánchez P, Ridao MA. Optimal management of microgrids with external agents including battery/fuel cell electric vehicles. IEEE Trans Smart Grid. 2019;10(4):4299–308. doi:10.1109/TSG.2018.2856524.
11. Xiao J, Wang P, Setyawan L. Multilevel energy management system for hybridization of energy storages in DC microgrids. IEEE Trans Smart Grid. 2016;7(2):847–56. doi:10.1109/TSG.2015.2424983.
12. Ravada BR, Tummuru NR, Ande BNL. Photovoltaic-wind and hybrid energy storage integrated multisource converter configuration-based grid-interactive microgrid. IEEE Trans Ind Electron. 2021;68(5):4004–13. doi:10.1109/TIE.2020.2984437.
13. Patel S, Ghosh A, Ray PK, Gurugubelli V. Effective power management strategy and control of a hybrid microgrid with hybrid energy storage systems. IEEE Trans Ind Appl. 2023;59(6):7341–55. doi:10.1109/TIA.2023.3303862.
14. Chen L, Wang X. Enhanced MPPT method based on ANN-assisted sequential Monte–Carlo and quickest change detection. IET Smart Grid. 2019;2:635–44. doi:10.1049/iet-stg.2019.0012.

15. Sumarmad KAA, Sulaiman N, Wahab NIA, Hizam H. Microgrid energy management system based on fuzzy logic and monitoring platform for data analysis. Energies. 2022;15(11):4125. doi:10.3390/en15114125.
16. Chakraborty S, Mehta P, Bharadwaj P. Smart hybrid energy management system for AC microgrid integrated to utility distribution grid. In: Proceedings of the 2024 IEEE 4th International Conference on Sustainable Energy and Future Electric Transportation (SEFET); 2024 Jul 31–Aug 3; Hyderabad, India. p. 1–6. doi:10.1109/SEFET61574.2024.10718209.
17. Khalid M, Panigrahi BK. Decentralized power management in multi BESS-PV based charging infrastructure for EV with SoC balancing. IEEE Trans Ind Appl. 2023;59(6):7392–403. doi:10.1109/TIA.2023.3305318.
18. Jayasinghe H, Gunawardane K, Zamora R. Multi-objective optimisation framework for standalone DC-microgrids with direct load control in demand-side management. Electron Lett. 2024;60(15):e13290. doi:10.1049/ell2.13290.
19. Chakraborty S, Mehta P, Bharadwaj P. Smart hybrid energy management system for green microgrid with optimized energy and enhanced voltage stability. IEEE Trans Ind Appl. 2025;61(6):8418–29. doi:10.1109/TIA.2025.3571335.
20. Zheng S, Liao K, Yang J, He Z, Sun X. A novel bilayer coordinated control scheme for global autonomous economic operation of islanded hybrid AC/DC microgrids. IET Renew Power Gener. 2021;15(12):2726–39. doi:10.1049/rpg2.12198.
21. Malik SM, Xin A, Sun Y, Chen Z, Zhou S. Voltage and frequency control strategies of hybrid AC/DC microgrid: a review. IET Gener Transm Distrib. 2017;11(2):303–13. doi:10.1049/iet-gtd.2016.0791.
22. Jafari M, Malekjamshidi Z, Lu DD, Zhu J. Development of a fuzzy-logic-based energy management system for a multiport multioperation mode residential smart microgrid. IEEE Trans Power Electron. 2019;34(4):3283–301. doi:10.1109/TPEL.2018.2850852.